Experimental observations of non-Gaussian behavior and stringlike cooperative dynamics in concentrated quasi-two-dimensional colloidal liquids

Andrew H. Marcus
Department of Chemistry and Materials Science Institute, University of Oregon, Eugene, Oregon 97403

Jeremy Schofield
Department of Chemistry, University of Toronto, Toronto, Ontario, Canada M5H 3H6

Stuart A. Rice*
The James Franck Institute, The University of Chicago, Chicago, Illinois 60637

(Received 3 May 1999)

We report, from direct observation of particle trajectories as a function of time, the presence of stringlike cooperative motion in a quasi-two-dimensional liquid. We have used digital video microscopy to study the equilibrium dynamics of suspensions of sterically stabilized uncharged poly(methylmethacrylate) spheres confined in a thin glass cell. Our experiments reveal the existence, in semidilute and dense liquid states, of a transition in the qualitative dynamical behavior of the system. At short times particles undergo unhindered Brownian motion, at intermediate times they undergo uncorrelated binary collisions, and at long times these one-particle self-diffusive modes are coupled to collective longitudinal acoustic modes of the fluid, the signature of which is local fluctuating domains of enhanced particle mobility. We study the properties of these domains by examining the density dependence of the van Hove self-correlation function and its deviation from Gaussian behavior. We observe that periods of non-Gaussian behavior correlate precisely with the timing of events involved in the relaxation of ''caged'' particles and their nearest neighbors. In contrast with relaxation processes in supercooled liquids, the lifetime of dynamical heterogeneities in a dissipative colloidal suspension is found to shift towards shorter time scales with increasing particle density. During time periods for which a quasi-two-dimensional system follows Gaussian behavior, we observe that, as predicted by Cichocki and Felderhof [J. Phys. Condens. Matter **6**, 7287 (1994)], the time dependence of the evolution of the effective diffusion coefficient from its short time to its long time value has the form $(\ln t)/t$. This last finding is true for all observed particle densities. To our knowledge, these results are the first experimental verification of the existence of microscopic cooperativity and the predicted temporal evolution of the diffusion coefficient for Brownian motion in concentrated quasi-two-dimensional liquids. [S1063-651X(99)06311-4]

PACS number(s): 82.70.Dd, 66.10.Cb, 66.20.+d

I. INTRODUCTION

Although much progress has been made in the theoretical description of dense molecular liquids, many of the microscopic details of the density dependence of the relaxation processes that occur are not completely understood. An improved theoretical understanding of the relative importance of individual particle and collective particle motion in the liquid state can potentially lead to significant advances in our understanding of the dynamics of supercooled liquids, the nature of viscoelasticity, and self-assembly in complex fluids [1].

Intuitively, it is clear that cooperative motion is an important contributor to the dynamics of dense Newtonian liquids. At low densities a molecule may move a distance of many diameters without hindrance from surrounding molecules, and one expects that large translational displacements are uncorrelated. At high densities, however, the lack of vacancies in the first-neighbor shell surrounding a molecule inhibits its large displacements, and local rearrangements can only occur through the correlated motion of many particles along pathways that preserve the local continuity of the system. Such local rearrangements typically occur in domains which are temporarily more ''fluidized'' than the background [2]. A given molecule will undergo small-amplitude ''vibrations'' inside its locally caged environment until thermal fluctuations create a fluidized domain in the molecule's immediate vicinity. Structural excitations, which create regions of greater diffusivity than the solidlike matrix of the surroundings, may give rise to a stringlike hopping transport mechanism. Until now, cooperative motion of this kind has only been observed directly in computer simulation [3].

The effects of cooperative motions on the dynamics of a system are described by mode-coupling theories in which multilinear combinations of collective excitation modes are coupled to molecular motion. The most important of these collective excitations forms a band of short-wavelength, self-diffusion-like generalized heat modes [4], which decay much more slowly than the other short-wavelength dynamical modes of the system, particularly for wavelengths comparable to the length scale of the nearest-neighbor separation. One of the successes of mode-coupling theory is the prediction, in dense liquids near the fluid-solid transition, of a distinct separation of relaxation time scales, specifically a slow global relaxation identified as the α-relaxation process and

*Author to whom correspondence should be addressed.

an intermediate rate relaxation as the β-relaxation process. Although the α-relaxation process is loosely associated with the rate-limiting structural relaxation of a molecular cage [5], until now there has been no direct experimental observation that links cage relaxation to the α relaxation. In this paper, we report experimental evidence that supports this intuitive, although admittedly oversimplified, mode-coupling picture for the α- and β-relaxation processes in a confined complex fluid.

Unlike a single-component Newtonian fluid, a colloidal suspension consists of interacting Brownian particles continuously subjected to the thermal fluctuations of the solvent bath. The viscous drag forces experienced by the particles rapidly regenerate the equilibrium distribution function of the colloid particles. Because of the dissipative nature of colloidal systems, momentum transfer between particles through inelastic collisions is expected to be less efficient than in a Newtonian fluid, and mode-coupling effects are also expected to be less important. For this reason, it is not obvious that one should be able to observe collective excitations in colloidal suspensions at all. Nevertheless, we show below that collective motion is an important aspect of colloid suspension dynamics and that its physical origin, viscoelastic coupling between self-diffusion-like heat modes and collective longitudinal acoustic modes, is very different from that of its Newtonian fluid counterparts.

This paper reports the results of dynamical studies of suspensions of uncharged colloidal spheres in a very thin cell. The experimental setup enables an individual particle and its surrounding cage of particles to be tracked through discrete time steps, which allows useful dynamical correlation functions to be easily calculated. The same experimental system has been used to study the equilibrium behavior of quasi-two-dimensional liquids [6,7] and the transport properties of a confined semidilute colloidal suspension [8]. In the limit in which hydrodynamic interactions can be treated as instantaneous and mode-coupling effects can be neglected, the evolution of this system can be described by a generalized Smoluchowski equation. We refer to this model system as a Smoluchowski liquid. Even in the absence of correlated particle motion, the diffusion coefficient for a Smoluchowski liquid has interesting properties. The value of the zero wave-vector diffusion coefficient is time-dependent by virtue of the difference between the two- (Brownian) particle equilibrium distribution function and the two-particle distribution function modified by the presence of a steady-state flow. In the short-time limit, that diffusion coefficient is determined by an integral of hydrodynamic interaction functions weighted by the equilibrium two-particle distribution function [9]. In the long-time limit the value of the colloid diffusion coefficient is determined by an integral of hydrodynamic interaction functions weighted by the radial part of the solution to the two-particle Smoluchowski equation [10].

In a two-dimensional Smoluchowski liquid, the asymptotic value for the diffusion coefficient of the Brownian particle is reached very slowly. Indeed, Cichocki and Felderhof recently investigated the self-diffusion in a semidilute suspension of interacting Brownian particles using the adjoint Smoluchowski operator to generate time displacements in the long-time regime [11]. In their treatment, they ignored both mode-coupling effects of the bath (which lead to divergence of the diffusion coefficient for a strictly two-dimensional liquid) and correlated collisions among the Brownian particles. They found that the mean-squared displacement $W(t)$ behaves for long times t as

$$W(t)=D_S^L t+(D_S^S-D_S^L)\tau_L \ln(t/\tau_M)+o(1), \qquad (1.1)$$

where D_S^L and D_S^S are the long- and short-time self-diffusion constants and τ_L and τ_M are time scales that depend on both the nature of the interactions between Brownian particles and the volume fraction of the suspension. They claim that the logarithmic term in Eq. (1.1) is due to a $1/t$ singularity in a memory function that is characteristic of Brownian systems in two dimensions, and hence Eq. (1.1) should apply for two-dimensional systems at any concentration. Recently, the validity of the functional form displayed in Eq. (1.1) for concentrated quasi-two-dimensional hard-sphere fluids was verified using a theoretical analysis that incorporated the effects of both mode coupling and binary uncorrelated collisions of the colloidal particles on the memory function describing the Brownian dynamics [12]. The system studied by Schofield, Marcus, and Rice differs somewhat from that studied by Cichocki and Felderhof. The system studied by the former investigators consisted of large hard spheres (the colloid particles) constrained to move in two dimensions, suspended in a fluid of small hard spheres that were allowed full three-dimensional motion. The system studied by the latter investigators consisted of large hard disks constrained to move in a two-dimensional continuum fluid. While the Schofield-Marcus-Rice calculations lead to the functional form displayed in Eq. (1.1), the coefficients found differ from those found by Cichocki and Felderhof. Prior to the work reported in this paper, to our knowledge there has not been an experimental verification of Eq. (1.1) at high concentrations.

The logarithmic term in Eq. (1.1) can be studied experimentally via examination of the effective self-diffusion coefficient defined by the ratio $\tilde{D}_S(t)=W(t)/t$. Making use of this definition and Eq. (1.1),

$$\tilde{D}_S(t)=D_S^L+(D_S^S-D_S^L)\tau_L\left[\frac{\ln(t/\tau_M)}{t}\right]+o(1). \qquad (1.2)$$

Equation (1.2) describes the long-time asymptotic behavior of the diffusion coefficient. The $(\ln t)/t$ functional form is predicted to be independent of particle interactions, at least for the case of short-range interactions, and is a signature of the solution to the two-dimensional Smoluchowski equation with direct particle-particle interactions.

Equations (1.1) and (1.2) have been observed to hold for semidilute ($\rho^*=\rho\sigma^2\sim 0.01$) quasi-two-dimensional suspensions of uncharged colloidal particles [7]. In those experiments, the single-particle (self)-dynamical correlation functions were well described by Gaussian distributions (consistent with the so-called Gaussian approximation) over the time periods for which the $(\ln t)/t$ form was observed. In Fig. 1 we display (a) a typical particle configuration with $\rho^*=0.01$, (b) particle trajectories representing a sequence of 40 time steps (1320 ms, 1 time step = 33 ms), (c) particle self-displacement histograms that are well fit to Gaussian spatial distributions, and (d) a plot of the mean-square displacement

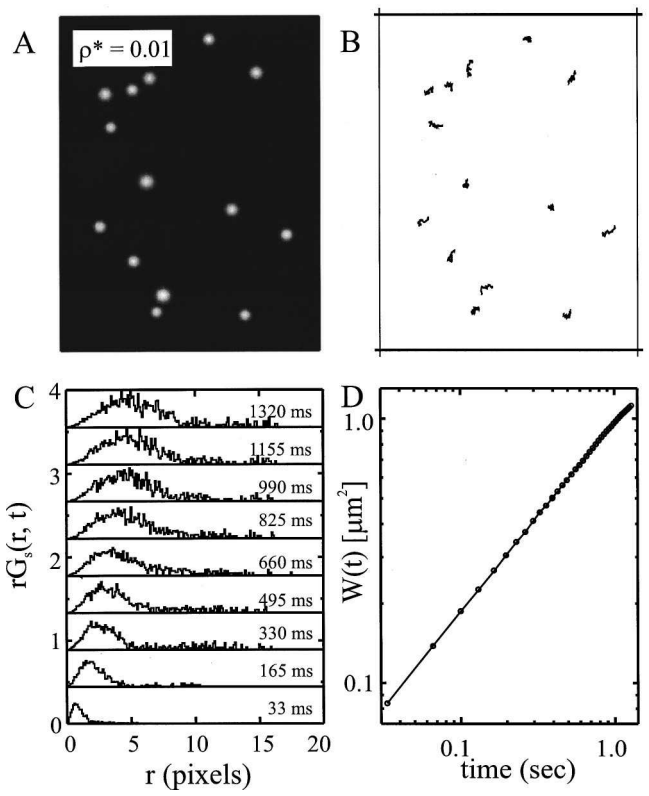

FIG. 1. (a) Typical particle configuration with $\rho^*=0.01$, (b) particle trajectories representing a sequence of 40 time steps (1320 ms, 1 time step = 33 ms), (c) particle self-displacement histograms that are well fit to Gaussian spatial distributions, and (d) a plot of the mean-square displacement (given by $W(t)=[\mathbf{r}_1(t)-\mathbf{r}_1(0)]^2/4$) that increases as a linear function of time for short times. Brownian particle mode-coupling effects are not observed in this low-concentration sample.

(given by $W(t)=[\mathbf{r}_1(t)-\mathbf{r}_1(0)]^2/4$) that increases as a linear function of time for short times. Hence, Brownian particle mode-coupling effects were not present in the low-concentration studies. We show below that Eqs. (1.1) and (1.2) correctly describe the dynamics of a quasi-two-dimensional colloid system over a wide range of particle densities, and over time periods for which the Gaussian approximation accurately describes the single-particle dynamical correlation functions. When the dynamical correlation functions become markedly non-Gaussian, mode-coupling effects become important and Eqs. (1.1) and (1.2) do not provide a useful representation of the dynamics.

II. EXPERIMENTAL METHODS AND CONSIDERATIONS

The procedure used to prepare monolayer colloidal suspensions and to construct the experimental glass cells was described in our previous papers [6–8]. Details specific to the work reported in this paper are given below. The diameter of the *PMMA* particles was determined to be $\sigma = 0.928\,\mu$m by scanning electron microscopy. These measurements also confirmed that the particle size distribution was monodisperse to within 1%. The surface of each particle was covered with an ~300-Å oligomeric brush of poly(3-hydroxystearate) that acts to sterically stabilize it with respect to aggregation induced by van der Waals forces. The *PMMA* particles were suspended in an aqueous sucrose solution (10% by weight) to reduce sedimentation, and confined between the walls of a thin glass cell. The cell walls were coated with trihydroxyoctadecylsilane (Huls-Petrarch), which acts to prevent adsorption of *PMMA* particles to the walls. The spacing between the cell walls could be varied and, for the experiments reported, was set to approximately 1.2 particle diameters (~ 1.2 μm). This thin cell configuration constrains the *PMMA* particle centers to a plane within a small fraction of a particle diameter; we determined by direct microscopic examination that the *PMMA* particle centers were coplanar to within the depth of focus of the objective (~0.25 μm). When the wall separation was smaller than ~1.2 μm, the particles were observed to be immobilized in the plane; when the wall separation was larger than ~1.2 μm, the particles were observed to have out-of-plane motion. No pathological effects were observed when the cell wall spacing was set to ~1.2 μm. The properties of these geometrically confined suspensions were studied over the two-dimensional reduced density range $\rho^*=0.01-0.93$.

The digital video microscopy (DVM) measurements were made using an Olympus BH3 metallurgical microscope with a 100×, numerical aperture 1.2, oil immersion objective. As already noted, the objective's depth of focus is a fraction of the *PMMA* sphere diameter, so that nonplanar particle configurations were easily detected. Images of the suspension were captured using a Hitachi charge-coupled device (CCD) video camera mounted to the microscope eyepiece. The frame frequency of the CCD camera was 30 Hz, while its shutter speed was $\frac{1}{100}$ s. The analog camera output was sent directly to the video port of a Silicon Graphics (SGI) Indy workstation. The SGI framegrabber supplied with the workstation was used to digitize sequences of 320×240 square pixel frames. A typical run consisted of 100 frames in sequence, corresponding to roughly 25 Mbytes of data. All image-processing procedures were implemented using IDL (Research Systems, Inc.), a programming language optimized for visual data analysis. The pixel length was calibrated by imaging a transmission electron microscope (TEM) grid of known scale. The aspect ratio was determined to be 1 ± 0.1 and the calibrated pixel dimension was 1 pixel $= 0.174\pm0.0015\,\mu$m.

A detailed description of the precision with which particle position can be measured in these experiments can be found in our previous papers [7,8] and the work of Crocker and Grier [13]. Briefly, the center-of-mass positions were determined with 0.1 pixel precision; the precision of center-of-mass location was thus 17.4 nm. The precision of the particle location is sufficient to calculate the mean particle density (using the number of particles in the frame and the pixel-to-length calibration) and the spatial correlation functions with much greater accuracy than is reported in any of our tables.

The observable in the DVM experiment is a complete set of two-dimensional N-particle trajectories, which can be combined to define the time-dependent density

$$\rho(\mathbf{r},t)=\sum_{i=1}^{N}\delta(\mathbf{r}-\mathbf{r}_i(t)). \tag{2.1}$$

The process of transforming the information contained in a sequence of digitized images into the time-dependent density

TABLE I. Thermodynamic states of experimental samples. The frame area A is 320×240 pix^2 (2219.5 μm^2). The areal density is measured in units of particle number per frame area normalized by the particle diameter ($\rho^*=N\sigma^2/A$, where $\sigma=0.928\,\mu$m). The assignments of the thermodynamic state were made in Ref. [8].

ρ^*	Number of particles inside field of view	Thermodynamic state
0.16	426	Dilute liquid
0.24	622	Dilute liquid
0.50	1300	Liquid
0.58	1498	Dense liquid
0.69	1775	Liquid-hexatic coexistence
0.83	2142	Hexatic
0.86	2208	Hexatic-solid coexistence
0.87	2247	Solid

profile described by Eq. (2.1) is discussed in our previous paper [7]. Given the trajectory data, it is a straightforward, though numerically taxing, application of statistical mechanics to calculate either static or dynamic spatial correlation functions of interest.

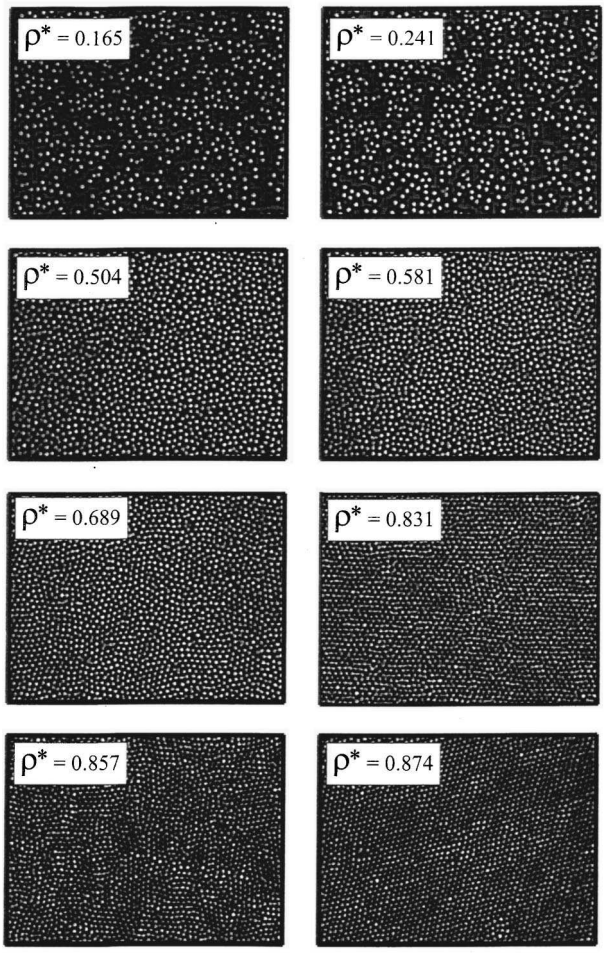

FIG. 2. Sample particle configurations of the quasi-two-dimensional assembly of *PMMA* spheres with frame size $56\times41\,\mu$m^2 and reduced density $\rho^*=0.165-0.874$. Each frame represents an equilibrium state of the system (see Table I).

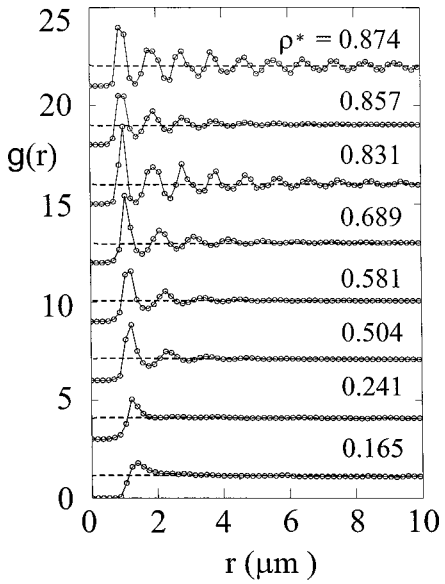

FIG. 3. Density dependence of the translational pair correlation function $g(r)$. The identities of the thermodynamic phases are listed in Table I. Positional order in the fluid phases is seen to decay exponentially with increasing particle separation.

III. EXPERIMENTAL OBSERVATIONS

Table I lists the different sample densities used in our investigations and the thermodynamic states we have assigned to them. Figure 2 displays sample configurations at each of these densities. Proceeding from the lowest to the highest density samples, the system has been studied in (i) pure liquid states ($\rho^*=0.165$, 0.241, 0.504, and 0.581), (ii) a state with coexistence between liquid and hexatic phases ($\rho^*=0.689$), (iii) a pure hexatic state ($\rho^*=0.831$), (iv) a state with coexistence between hexatic and solid phases ($\rho^*=0.857$), and (v) a pure solid state ($\rho^*=0.874$).

The identities of the pure two-dimensional phases existing at the densities examined in this work were established by computing the static correlation functions from statistical averages of the particle positions. The details of this analysis are presented in our previous papers [7,8]. In Fig. 3 are shown the results of our analyses of the respective pair correlation functions. These results provide conclusive evidence for the assignments of the character of the pure fluid phases mentioned above; the positional order in the fluid phases is seen to decay exponentially with increasing particle separation. The translational correlation functions were obtained by computing histograms of the measured distribution of particle separations from [14]

$$g(r)=\rho^{-2}\left\langle \sum_i \sum_{j\neq i} \delta(\mathbf{r}_i)\,\delta(\mathbf{r}_j-\mathbf{r}) \right\rangle. \tag{3.1}$$

We note that the state with hexatic-solid coexistence ($\rho^*=0.857$) exhibits a translational correlation length shorter than either the pure hexatic ($\rho^*=0.831$) or the pure solid ($\rho^*=0.857$) states.

We observe that even for the lowest density samples almost every particle is in close proximity to at least one adjacent neighbor (see Fig. 2). This observation is consistent with the conclusion of our structural studies, namely that

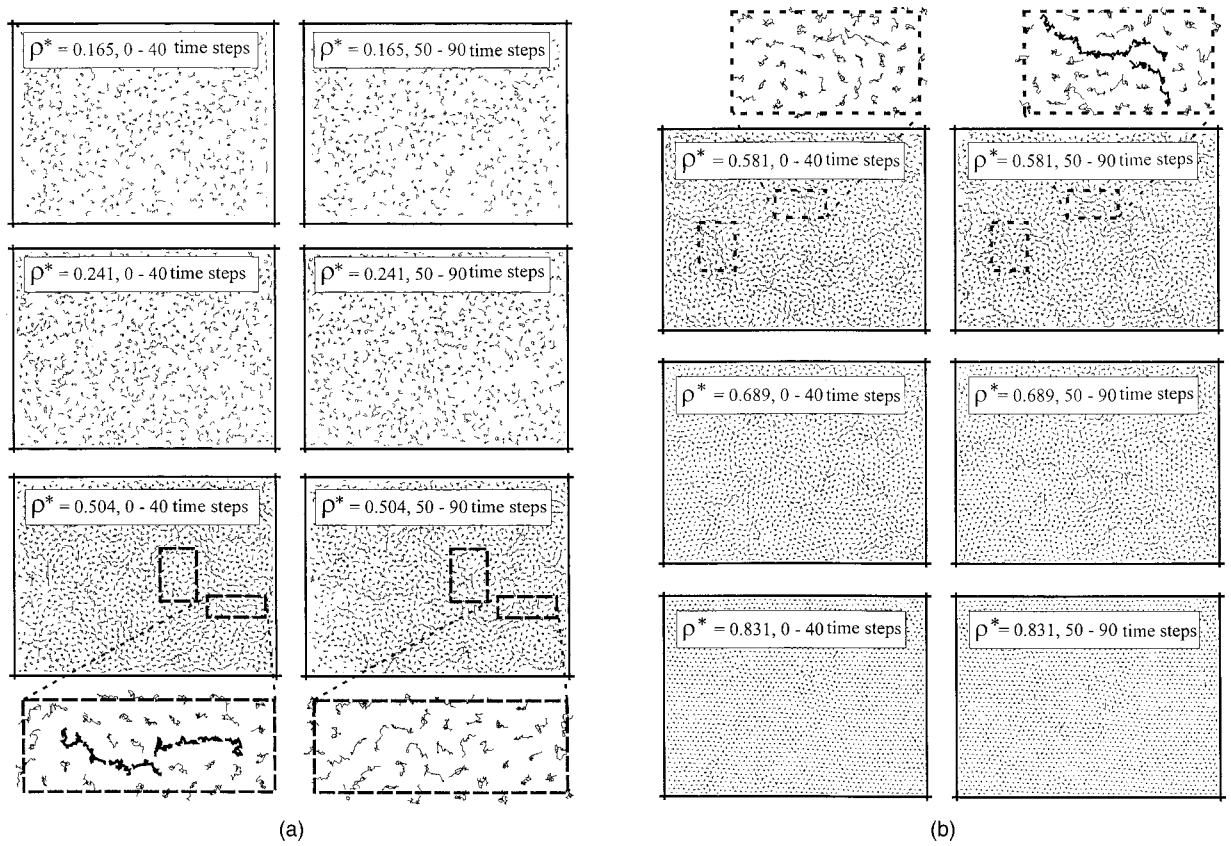

FIG. 4. (a) and (b) Particle trajectories as a function of density. Line segments connect the particle positions between successive video frames. The duration of these sequences is for 40 frames or for 1320 msec. At each density, two successive 40 frame sequences are shown. The effects of dynamic heterogeneity and cooperative motion are most apparent for the samples with densities $\rho^* = 0.504$ and 0.581. Expanded views show local particle regions where the dynamic behavior alternates between confined motion and cage relaxation through cooperative long-range jumps.

there is a weak attractive component ($\sim 1 k_B T$) to the short-range interparticle interaction potential [6,8]. We also note that for the lowest density sample ($\rho^* = 0.165$) at any given instant, most of the particles appear to be connected into stringlike clusters. This tendency to form isolated strings is less pronounced as the density is increased. However, it is shown below that stringlike features *in the dynamics* appear at higher densities.

A key element in the study of two-dimensional colloidal suspensions is the establishment of equilibrium. In the systems we studied it was possible to prepare monolayer suspensions with more than 10^6 particles with a uniform number density. We required that consistent and reproducible results be achieved by recording data over a 72–168-h period at each sample density. Further evidence that the results reported in this work are equilibrium properties of the colloid suspension is provided by our observation that the systems appear to exhibit ergodic behavior. In Figs. 4(a) and 4(b) are plotted trajectory maps of particle displacements corresponding to the first six particle densities shown in Fig. 2. Each map consists of 40 sequentially linked particle positions so that the full time duration is 1320 ms(1time step = 33 ms). When $\rho^* = 0.504$, 0.581, and 0.689, particles are spatially segregated into two subpopulations: those that undergo Brownian motion within pseudohexagonally ordered clusters and those that appear to move freely in stringlike channels about the edges of these clusters. For each density, a comparison is shown between the trajectory maps constructed from the first 40 frames (sequence 0–40) and those of the last 40 frames (sequence 50–90) of a 90-frame sequence. The magnified insets for $\rho^* = 0.504$ and 0.581 illustrate the transient nature of the dynamic heterogeneity. Although the particles are always partitioned between mobile and immobile subpopulations, the identities of the particles assigned to either group change in time, thereby demonstrating that fluidized domains exist in this system as a consequence of natural collective fluctuations of the colloidal liquid. This observation is consistent with the interpretation that the suspensions exhibit ergodic behavior.

To qualitatively examine the range of dynamical behavior exhibited by a tagged colloidal particle, we isolated single-particle trajectories consisting of 150 time steps (= 4950 ms) for each sample density. Figure 5 shows some typical plots of single-particle trajectories corresponding to the six lowest densities. The dotted circles indicate the size and positions of the particles in the final frame of the trajectory sequence. The most striking feature of these trajectories is that there are transient periods of small-amplitude motions followed by periods of large-amplitude displacements that occur at all but the highest particle densities shown. Even for the lowest sample densities ($\rho^* = 0.165$ and 0.241) this behavior, indicative of structural relaxation (the so-called cage effect), is apparent. We attribute this behavior to a cooperative jump mechanism that is operative over the full range of fluid

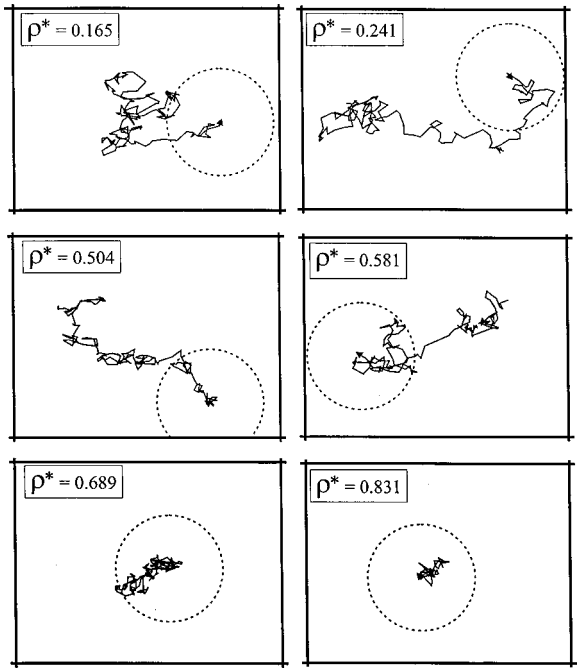

FIG. 5. Single-particle trajectories as a function of density. The dotted circles indicate the size and positions of the particles in the final frame of the trajectory sequence. Transient periods of small amplitude motions are followed by periods of large amplitude displacements for all but the highest particle densities shown.

sample densities we have studied. The origin of cooperative jumps in this system is discussed in more detail below.

From Figs. 4(a) and 4(b) it can be seen that at intermediate densities ($\rho^*=0.504$, 0.581, and 0.689), long-range displacements occur in cooperative stringlike patterns. This mode of motion arises because the occurrence of a long-range jump is usually closely associated with a similar event involving a nearest-neighbor particle. In Fig. 6, the relationship between the displacements of a tagged particle and its cage of nearest neighbors is examined more closely. The trajectories of a local particle configuration corresponding to a typical long-range jump event ($\rho^*=0.581$) are plotted for three sequential 20-frame (660 ms) sequences. As in the preceding figure, the dashed circles indicate particle size and positions at the end of each trajectory. In the first 20 time steps of the sequence the particles undergo local motion within their individual cages. In frame sequence 20–40 an initially caged particle (colored red) is seen to make a large displacement to a nearest-neighbor site. During the same time interval, a neighboring particle (colored green) makes a large displacement and replaces the red particle in its initial position. The final 20-frame sequence shows that these two particles continue to undergo localized motion after the cooperative jumps have occurred. The time interval separating periods of localized motion is 20 frames (or 660 ms) indicating that, for $\rho^*=0.581$, the late stages of the breakdown of the cage occur on this time scale.

The generality of the above observations can be examined by considering the self-part of the van Hove correlation function, $G_s(r,t)$, defined as [14]

$$G_s(r,t)=\frac{1}{N}\left\langle \sum_{i=1}^{N} \delta(r-|\mathbf{r}_i(0)-\mathbf{r}_i(t)|)\right\rangle . \qquad (3.2)$$

$G_s(r,t)$ is the probability that a particle has suffered a displacement, r, in the time interval t. If $G_s(r,t)$ depends only on the magnitude of $\mathbf{r}$, it is sufficient to examine $2\pi r G_s(r,t)$. Figure 7 shows plots of $rG_s(r,t)$ constructed from particle trajectories that correspond to the sample densities examined in this work. We first examine the lowest density sample with $\rho^*=0.165$. $G_s(r,t)$ is at short times a single-mode, approximately Gaussian, distribution with a second moment (given by $W(t)=\langle[\mathbf{r}_1(t)-\mathbf{r}_1(0)]^2\rangle/4$) that increases as a linear function of time. This is consistent with the interpretation that at this density, and at very short times, the particles primarily undergo independent Brownian motion with diffusion coefficient, D_S^S. At intermediate times the particles begin to experience uncorrelated binary collisions with their nearest neighbors. The effect of these random collisions is to modify the diffusion coefficient at intermediate times to a smaller value than D_S^S. During the intermediate time regime, $G_S(r,t)$ remains essentially a Gaussian spatial distribution, although its second moment, $W(t)=\tilde{D}_S(t)t$, increases in time more slowly than it does at short times [i.e., $\tilde{D}_S(t)<D_S^S$]. On this intermediate time scale, the time-dependent functional form of $W(t)$ follows Eq. (1.1), indicative of a transition from ''free''-particle diffusion to a modified diffusion that is effectively ''dressed'' by in-plane random binary collisions. We further examine the density

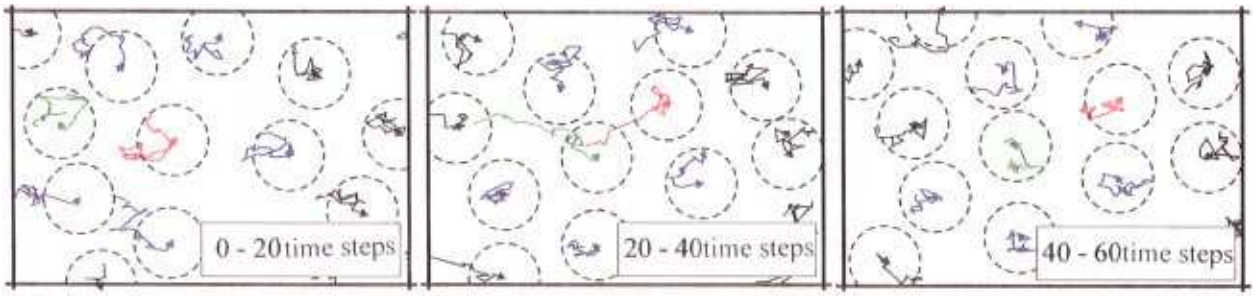

FIG. 6. (Color) Relationship between the displacements of a tagged particle and its cage of nearest neighbors. The dashed circles indicate particle size and positions at the end of each trajectory. Successive 20 frame sequences show (i) particles undergoing local motion within their individual cages, (ii) an initially caged particle (colored red) executing a large displacement to a nearest-neighbor position while a neighboring particle (colored green) replaces the red particle in its initial position, followed by (iii) localized motion after the cooperative jumps have occurred.

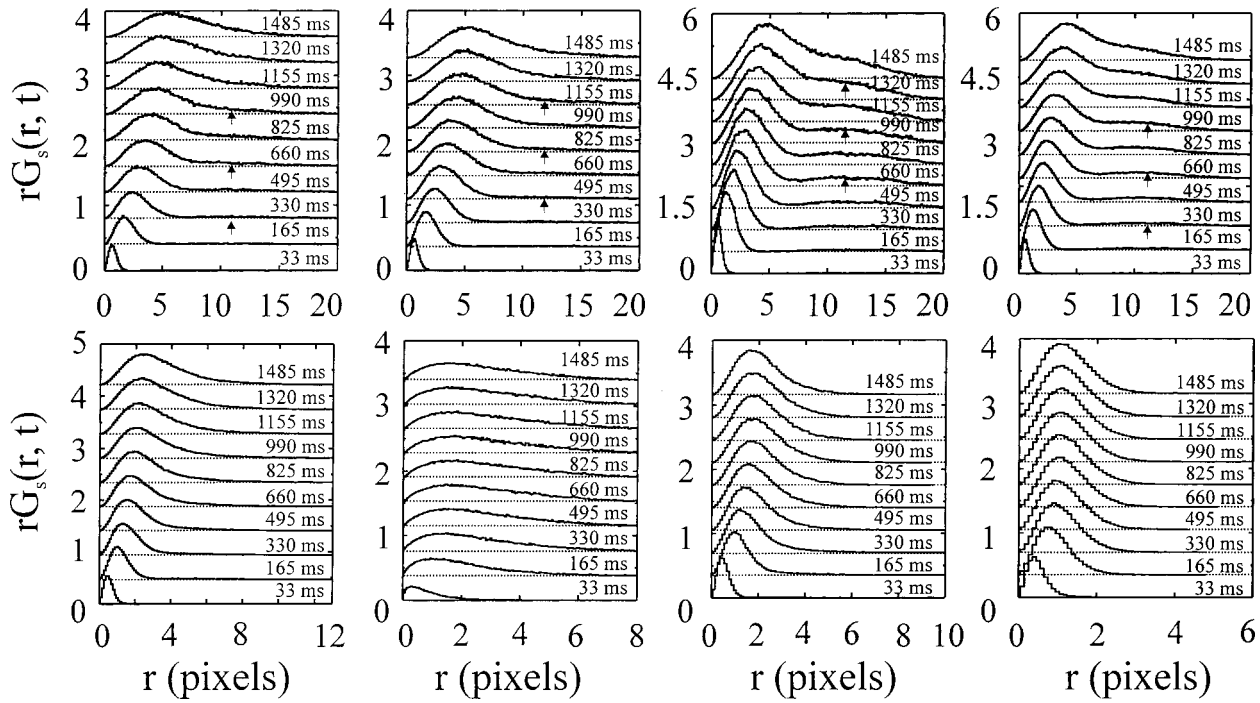

FIG. 7. Density dependence of the van Hove self-correlation function $rG_s(r,t)$ constructed from particle trajectories according to Eq. (3.2). The physical units of the horizontal axes are in pixels (0.174 μm/pixel). Densities are from left to right, top to bottom: $\rho^*=0.165$, 0.241, 0.504, 0.581, 0.689, 0.831, 0.857, and 0.874. Arrows indicate non-Gaussian features (described in text).

dependence of the particle dynamics in the random binary collision regime in our discussion of the behavior of $\tilde{D}_S(t)$ below.

At longer times, and still for the lowest sample density, $\rho^*=0.165$, a non-Gaussian ''tail'' can be seen to develop in $G_s(r,t)$ for $t\geqslant 330$ ms (indicated by arrows in Fig. 7). Similar behavior is also found for $\rho^*=0.241$. These tails in the distribution functions are due to the occurrence of long-range cooperative hops. At these low densities the tail is neither prominent nor localized to a narrow range of displacement values for the duration of the experiments. For $\rho^*=0.504$ and 0.581, the hopping effect is more pronounced; a broad but distinct secondary peak in $G_s(r,t)$ (indicated by arrows) appears at a distance equal to the average separation between a particle and one of its nearest neighbors. When $\rho^*=0.504$, the secondary peak has its maximum value when $t\sim 1155$ ms, while for $\rho^*=0.581$ the secondary peak is a maximum when $t\sim 660$ ms. We note that these secondary peaks in the distributions $G_s(r,t)$ would not be present unless the long-range hops occur in a cooperative fashion. That is, within a time period in which a particle undergoes a long-range displacement, there is a high probability that another nearby particle will also undergo a long-range displacement. Cooperative motion, in this sense, is a good description of the trajectory data shown in Figs. 4, 5, and 6, and as discussed above, these jumps occur in stringlike patterns.

For all sample densities that are greater than $\rho^*=0.581$, $G_s(r,t)$ is again a single-mode distribution for the duration of the experiments. When $\rho^*=0.689$, and for $t\geqslant 1320$ ms, the curves show a tendency to cluster around displacements in the range $0.15\leqslant r\leqslant 0.9\,\mu$m. The same effect can be seen for $\rho^*=0.831$ and $165\leqslant t\leqslant 1485$ ms, for which clustering occurs around $0.15\leqslant r\leqslant 0.7\,\mu$m. As with the lowest density samples, the particle movement has slowed down significantly, thereby defining a structural arrest effective for the specified range of time and spatial scales. The distances over which this structural arrest occurs are small compared to the nearest-neighbor separation; thus the processes that occur in these time windows appear to be related to the evolution of the particle cages before their complete breakdown.

To examine more closely the time and spatial scales for which $G_s(r,t)$ deviates from Gaussian behavior, we calculated the non-Gaussian parameter from our data using the appropriate form for a two-dimensional fluid [15],

$$\alpha_2(t)=\frac{\langle[\mathbf{r}_1(t)-\mathbf{r}_1(0)]^4\rangle}{2\langle[\mathbf{r}_1(t)-\mathbf{r}_1(0)]^2\rangle^2}-1. \tag{3.3}$$

Figure 8 shows plots of α_2 as a function of particle density. The curve corresponding to $\rho^*=0.01$ was calculated from data taken from Ref. [7], a representative portion of which is shown in Fig. 1. For this very dilute sample, α_2 is less than 0.01 at all observed times. Although the higher concentration data are limited to the narrow window of the experimentally accessible time scale, it is possible to detect a systematic trend in the behavior of α_2; as the particle density is increased, the maximum value of α_2 tends to become larger while the time associated with the peak position tends to become smaller. We find that for the time domain for which particle motion is dominated by binary uncorrelated collisions, α_2 is nonzero but small. Upon entering the time domain for which particle motion is hindered by neighboring particles (the so-called β-relaxation regime), we expect α_2 to increase [3]. An increase in the value of α_2 is observed for $\rho^*=0.165$, 0.241, 0.504, and 0.581. However, for the first four densities the locations of the peak positions cannot be

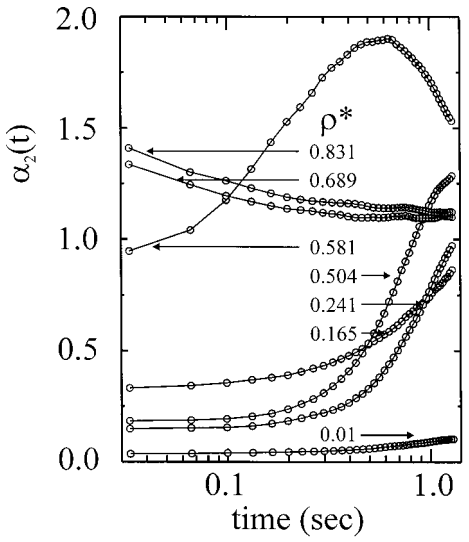

FIG. 8. Non-Gaussian parameter $\alpha_2(t)$ [Eq. (3.3)] plotted against a log base-e time axis. Curves are shown corresponding to the density range $\rho^* = 0.165 - 0.831$.

deduced from the recorded data. On the time scale for which cooperative motion is the most prominent mechanism of relaxation (the α-relaxation regime), we expect α_2 to decrease with increasing time. A decrease of the value of α_2 is observed for $\rho^* = 0.581$, 0.689, and 0.831. At very long time (the hydrodynamic limit), we expect α_2 to approach zero since in this limit $G_s(r,t)$ must return to Gaussian behavior. We note that the single plot of α_2 for which both the rise and fall of the peak can be resolved corresponds to the sample with density $\rho^* = 0.581$. This is the sample in which dynamic heterogeneity is most pronounced during our observation time window [see Fig. 4(b)], and in which the evolution of a particle and its cage of nearest neighbors can be completely followed (see Fig. 6). The time scale associated with a cooperative jump at this density (20 time steps=660 ms) corresponds precisely to the peak position of α_2 (see discussions of Figs. 6 and 7). The two highest sample densities ($\rho^* = 0.689$ and 0.831) show a steady decrease of the value of α_2 with increasing time. In this case, however, the decrease in α_2 does not necessarily indicate that the system is returning to Gaussian behavior since α_2 asymptotically approaches a sizable nonzero value. We return to this point below.

Non-Gaussian behavior of $G_s(r,t)$ has been observed in simulations of glass-forming liquids and it is thought that this behavior reflects the presence of dynamic heterogeneities in the system [3]. If we follow this interpretation, our data suggest that the dynamics of the liquid tends to become more heterogeneous as the density is increased. However, in contrast to the behavior of simulated supercooled liquids, the apparent lifetime of a dynamic heterogeneity (in this case, the inverse frequency of short-wavelength longitudinal acoustic modes) systematically decreases with increasing density.

For the lowest density sample examined ($\rho^* = 0.165$), the short-time behavior of α_2 indicates that the van Hove function is significantly non-Gaussian even for times much shorter than the onset of structural arrest or cage relaxation. The small magnitude of α_2 for very dilute samples ($\rho^* \leqslant 0.01$) is consistent with the Gaussian approximation as expected. Non-Gaussian behavior for $\rho^* = 0.165$ is consistent with our observations that stringlike particle configurations are predominant and can influence the dynamics even at this low density. The stringlike local configurations lead to a short-ranged and short-lived anisotropy of the liquid, which strongly inhibits short-time random isotropic particle motion. Hydrodynamic effects could also contribute to non-Gaussian behavior at these densities. As the density is increased ($\rho^* = 0.241$ and 0.504), short-time non-Gaussian behavior becomes less significant. For the two highest sample densities ($\rho^* = 0.689$ and 0.831) it is only possible to see α_2 gradually decrease from a maximum value that occurs on time scales much shorter than our experimental sampling time interval. According to our previous reasoning, this time interval should correspond to the α-relaxation regime, since α_2 is gradually decreasing. Indeed, it is possible to distinguish the weak signs of cooperative motion and heterogeneous dynamics from the trajectories corresponding to these densities [see Fig. 4(b)]. However, as noted above, at long times and for these densities, α_2 asymptotically approaches a constant nonzero value. This is consistent with our previous observation [see discussion of $G_s(r,t)$ and Fig. 7] that on these time scales a structural arrest appears to be taking place and that the system is exhibiting the dynamics characteristic of the β-relaxation regime. Thus, the interpretation of an apparent short-time peak in α_2 for the $\rho^* = 0.689$ and 0.831 samples is most likely unrelated to structural relaxation. It is possible that the apparent short-time peak at high density (and the nonzero value of α_2 at low density) is related to correlated particle motion due to the effects of hydrodynamic interactions. Solvent velocity fields surrounding a given particle are established much more rapidly than the experimental sampling time of our experiments ($\tau_H \sim \mu$ sec$\ll t_0 = 33$ msec). These hydrodynamic fields can, in principle, exert instantaneous nonrandom forces on neighboring particles thereby influencing their motion [14]. Such hydrodynamic effects should become progressively more important at high densities for which the time scale between colloid particle interactions is of the same order of magnitude as the propagation time of the hydrodynamic velocity fields over the average distance between particles. In this regime, dynamical correlations induced by the hydrodynamic flow may be important. A complete assessment of the relative importance of hydrodynamic contributions to the particle dynamics will be the topic of future reports [16].

We now examine the time dependence of the mean-square displacement, $W(t) = \langle [\mathbf{r}_1(t) - \mathbf{r}_1(0)]^2 \rangle / 4$. Figures 9(a) and 9(b) show this quantity evaluated from our data plotted on a base-e log-log scale. In Fig. 9(a), the y axis is given in an absolute scale so that the density dependence of the magnitude of $W(t)$ can be compared directly. In Fig. 9(b) the y axis is given in arbitrary units; $W(t)$ has been reduced in terms of pixels and individual curves have been offset in the vertical direction for clarity. Figure 9(b) compares the density dependence of the time-dependent slopes of $W(t)$. Table II lists the initial (m_1) and final (m_2) slopes of the fitted lines (dotted) as a function of particle density. For $0 \leqslant t \leqslant 66$ ms and $\rho^* = 0.165 - 0.689$, the data are well described by a diffusive process (the initial slopes are close to 1). At longer times the data fit a weaker than diffusive power law that we associate

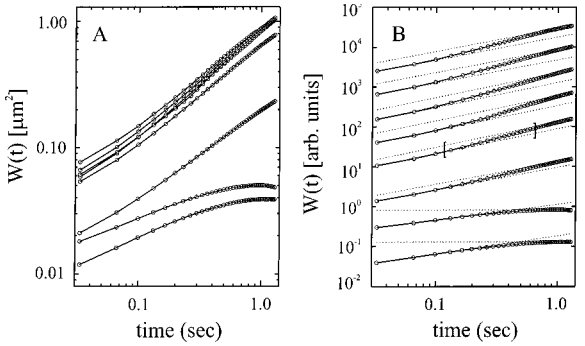

FIG. 9. (a) Time-dependent mean-square displacement, $W(t) = \langle [r_1(t) - r_1(0)]^2 \rangle / 4$, plotted on a base-$e$ log-log scale. Variations in curve shape occur systematically with increasing density from top to bottom: $\rho^* = 0.077$, 0.165, 0.241, 0.504, 0.581, 0.689, 0.831, and 0.874. Note that the curves with densities 0.241 and 0.504 lie almost on top of one another. (b) Variations in slope of mean-square displacement as a function of density. The y axis is given in arbitrary units; $W(t)$ has been reduced in terms of pixels and individual curves have been offset in the vertical direction for clarity. Curves are shown in order of increasing density from top to bottom. For $\rho^* = 0.581$, brackets are shown to indicate the time window during which a kinetic transition occurs. Initial (m_1) and final (m_2) slopes (dotted lines) are listed in Table II as a function of particle density.

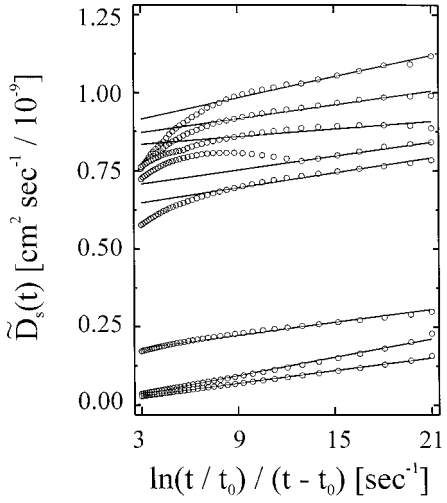

FIG. 10. $\tilde{D}_s(t)$ vs $\ln(t/t_0)/(t-t_0)$ as a function of particle density. The x axis has units of frequency and $t_0 = 1$ time step (33 msec). Table III lists values obtained from the linear fits (solid lines) to the short-time data. The y intercept is equal to the long-time self-diffusion coefficient D_S^L, while the slope $[(D_S^S - D_S^L)\tau_L]$ is the difference between the long- and short-time diffusion constants scaled by the constant τ_L [see Eq. (1.2)].

with the cooperative processes that define the α-relaxation regime. For $\rho^* = 0.581$, there is a distinctive region (indicated by the brackets) where the change in slope levels off into a short plateau. This bracketed region corresponds to the time window for which α_2 rises to its peak value (see Fig. 8). For this time interval, there is an apparent arrest of the particle motion that is the signature of the β relaxation. We note that the long-range cooperative jumps occur at longer time than the β-relaxation window, and are correlated with the long-time α-relaxation processes. When $\rho^* = 0.831$ and 0.874, the onset of the plateau region in $\ln[W(t)]$ extends to the shortest observable time (since the initial slopes are less than 1). This is consistent with the interpretation that, at these densities, the particles are so highly confined that for the entire range of observable time the system is only observed in the β-relaxation regime.

We now compare the results of our experiments with the predictions of Cichocki and Felderhof [11]. As discussed in Sec. I and defined by Eq. (1.2), the quantity $\tilde{D}_S(t) = dW(t)/dt \approx [W(t) - W(t_0)]/(t - t_0)$ is a measure of the effective time-dependent self-diffusion coefficient. In Fig. 10 we display $\tilde{D}_S(t)$ versus $\ln(t)/t$ as a function of particle density. It has been shown theoretically [11,12] and experimentally [7] that for both a two-dimensional and a quasi-two-dimensional system of hard particles undergoing binary uncorrelated collisions, $\tilde{D}_S(t)$ has the time-dependent form $\ln(t)/t$. We note that the quantity $\ln(t)/t$ has units of frequency and that at high frequencies (or short times), within the precision of our data, the $\ln(t)/t$ behavior is observed for all of the densities examined. We interpret this result as evidence that at short times and for all densities, particle motion is well described by the Cichocki-Felderhof model of Brownian diffusion dressed by binary uncorrelated collisions. Note that our inference implies that our shortest period of observation is already in the asymptotic time regime for the temporal development of $\tilde{D}_S(t)$.

Table III lists values obtained from the linear fits (solid lines) to the short-time data shown in Fig. 10. According to

TABLE II. Slopes of short- and long-time linear fits to $\ln[W(t)]$ versus $\ln[t]$ corresponding to the dotted lines in Fig. 9(b).

ρ^*	m_1	m_2
0.16	0.9	0.9
0.24	0.9	0.9
0.50	1.0	1.0
0.58	1.0	1.0
0.69	1.0	1.0
0.83	1.0	1.0
0.86	0.4	0
0.87	0.3	0

TABLE III. Slopes and y intercepts of short-time linear fits for $[W(t) - W(t_0)]/(t - t_0)$ versus $\ln(t/t_0)/t$ (Fig. 10) as a function of areal density. ($t_0 = 33$ ms.)

	Short-time fits	
ρ^*	$(D_S^S - D_S^L)\tau_L$ (μm^2)	D_S^L (μm^2 sec^{-1})
0.16	0.021	0.086
0.24	0.013	0.084
0.50	0.043	0.083
0.58	0.017	0.070
0.69	0.014	0.061
0.83	0.012	0.016
0.86	0.023	0.00
0.87	0.015	0.00

TABLE IV. Characteristic time constants corresponding to short-time linear fits for $[W(t)-W(t_0)]/(t-t^0)$ versus $\ln(t/t_0)/t$, where $t_0=33$ ms (Fig. 10). Short-time fits are based on the assumption $D_S^S \approx D_0 = 0.185\ \mu\text{m}^2\ \text{sec}^{-1}$.

	Short-time fits		
ρ^*	τ_L (sec)	Δ (μm^2)	τ_M (sec)
0.16	0.21	0.023	0.33
0.24	0.13	0.015	0.32
0.50	0.42	0.0055	0.28
0.58	0.15	0.019	0.33
0.69	0.11	0.016	0.32
0.83	0.07	0.013	0.34
0.86	0.12	0.025	0.34
0.87	0.08	0.017	0.32

Eq. (1.2), the y intercept is equal to the long-time self-diffusion coefficient D_S^L, while the slope $[(D_S^S-D_S^L)\tau_L]$ is the difference between the long- and short-time diffusion constants scaled by the constant τ_L. The values obtained for D_S^L appear to decrease systematically with increasing particle density. These values of D_S^L are reached according to the form given by Eq. (1.2) over the time interval shown in Fig. 10 ($33<t<330$ ms). The short-time diffusion coefficient D_S^S could nominally be assigned the same value as the bare diffusion constant, namely, $D_0=0.521k_BT/6\pi\eta a = 1.85\times10^{-9}\ \text{cm}^2\ \text{sec}^{-1}$. This value is calculated from the Stokes-Einstein equation with the necessary correction to account for the hydrodynamic friction due to the effect of the cell walls [17]. It is evident from Fig. 10 that at the lowest sample density, and for the shortest time shown ($t=33$ ms), the diffusion coefficient has a value similar to, although slightly smaller than, our estimated D_0. Using this value for D_S^S, we calculated the time constants τ_L listed in the first column of Table IV. To determine τ_M, it is necessary to take the long-time limit of the difference equation [11],

$$\Delta = \lim_{t\to\infty}[W(t)-D_S^L t-(D_S^S-D_S^L)\tau_L \ln(t)] = -(D_S^S-D_S^L)\tau_L \ln \tau_M . \quad (3.4)$$

The values obtained for Δ using Eq. (3.4) are listed in the second column of Table IV. These values for Δ were used to determine τ_M through

$$\tau_M = \exp[-\Delta/(D_S^S-D_S^L)\tau_L]. \quad (3.5)$$

The values for τ_M are listed in the third column of Table IV. We note that τ_M appears to be independent of the particle density.

For the two-dimensional Smoluchowski liquid, $\tau_L \sim a^2/D_0 \cong 1$ sec. Thus the magnitude of the measured $(\ln t)/t$ term in Eq. (1.2) is approximately ten times smaller than in the theoretical prediction. Another inconsistency occurs between our data and the predictions of Ackerson and Fleishman for low densities (where mode-coupling effects were not included) [18], and between our data and the predictions of Schofield, Marcus, and Rice for all densities (where mode-coupling effects were included) [12]. Figure 11 displays values for the fractional area ($\phi=N\pi a^2/A$) and the predicted and experimental values of D_S^L/D_0 for each of the sample densities examined in this work. Corresponding values for ϕ and ρ^* are listed in Table V. At relatively low densities ($\rho^*=0.16$ and 0.24), the theoretically predicted long-time diffusion constant appears to overestimate the measured values by a factor of 1.5. At intermediate densities ($\rho^*=0.50$, 0.58, and 0.69), the theoretical predictions consistently underestimate the measured values. The theoretical predictions that include mode-coupling effects underestimate the measured values slightly more than do the predictions that ignore mode-coupling effects. At the highest densities ($\rho^*=0.83$, 0.86, and 0.87), the agreement between experiment and theory is much better. We note that at these densities, the theory that includes mode-coupling effects follows the experimental values more closely than do the theoretical predictions that do not include mode-coupling effects.

TABLE V. Comparison between the mean collision time $\langle\tau_{\text{collision}}\rangle$ and the experimentally observed density dependence of the peak positions of the non-Gaussian parameter $\alpha_2(t)$. The area fraction $[\phi=N\pi(\sigma/2)^2/A]$ is shown for the comparison with mode-coupling results in Fig. 11. ϕ is related to the reduced particle density through $\phi=(\pi/4)\rho\sigma^2=(\pi/4)\rho^*$.

ρ^*	ϕ	$\langle l_{\text{sep}}\rangle$ (μm)	$\langle\tau_{\text{collision}}\rangle$ (sec)	Experimental peak position of α_2 (sec)
0.16	0.13	2.17	6.2	>1.3
0.24	0.19	1.71	3.9	>1.3
0.50	0.39	1.02	1.4	~1.3
0.58	0.46	0.90	1.1	~0.7
0.69	0.54	0.76	0.8	Plateau region in $W(t)$
0.83	0.65	0.60	0.5	Plateau region in $W(t)$

It is possible that the disagreement between theory and experiment is due to systematic errors. A possible source of error is the estimated value of D_0, which depends on the sucrose concentration of the host solution; that concentration is estimated to be accurate within 1%, and we presume the tabulated viscosity of sucrose has the same accuracy. Our estimate of D_0 ($=k_BT/\xi$) also depends on the hydrodynamic correction due to wall effects ($\xi=\xi_0\times$correction factor). The wall spacing was determined to be 1.2 μm by visualizing defects on the walls. This measurement should have a precision of roughly the depth of focus of the objective, 250 nm, so we expect the error in the wall correction to the frictional force to be small ($\xi/\xi_0=1.92\pm0.25$). This leads to an uncertainty in the estimated value of $D_0=0.185\pm0.022\ \mu\text{m}^2\ \text{sec}^{-1}$. This uncertainty is reflected in the error bars shown in Fig. 11. Although there could be an unrecognized systematic error in our measurements, we do not believe this to be the case. It is important to note that an error in D_0 alone cannot account for the discrepancies in both D_S^L/D_0 and τ_L, since a variation in D_0 can only lead to improvement in one quantity at the expense of the other. The most probable explanation is that the idealized theoretical values obtained for the coefficients should not directly apply to our experimental system. This is not too surprising since the Cichocki-Felderhof analysis is based on a strictly two-dimensional system of colliding hard disks in the absence of

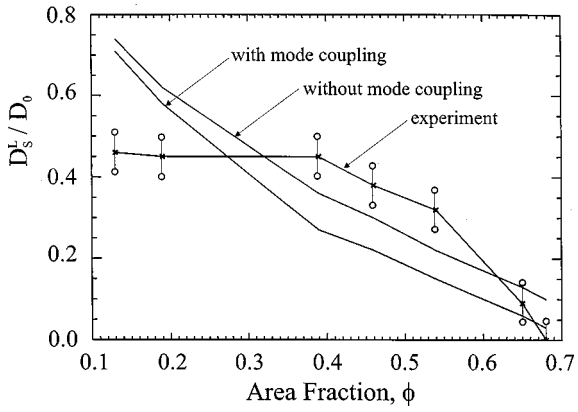

FIG. 11. Comparison between the experimentally determined values for the ratio of the long- and short-time diffusion constants, D_S^L/D_0, and the theoretical predictions for a strictly two-dimensional system of hard disks given by Schofield, Marcus, and Rice [12]. The fractional area of the plane covered by N disks of radius a is $\phi = \pi N a^2/A$.

hydrodynamic interactions, which is certainly very different from our quasi-two-dimensional colloidal suspension.

We now discuss the density-dependent behavior of $\tilde{D}_S(t)$ at long times (Fig. 10). For the two highest densities shown ($\rho^* = 0.857$ and 0.874), the $\ln(t)/t$ form persists for the full range of observed time scales. At these densities, the dynamics are dominated by binary uncorrelated collisions among particles that are frozen within arrested local environments and no cage relaxation is observed. For $\rho^* = 0.831$, we see a gradual change in the slope of the $\ln(t)/t$ dependence of $\tilde{D}_S(t)$ at the lowest observed frequencies. This indicates that on these time scales, and at this density, a structural barrier associated with the nearest-neighbor cage interrupts particle diffusion, causing $\tilde{D}_S(t)$ to decrease. Our previous observations of the van Hove self-correlation function, $G_s(r,t)$, and the mean-squared displacement, $W(t)$, show that structural relaxation is arrested at this density for this time domain. Similar behavior is observed for the sample with density $\rho^* = 0.689$. However, in this instance the decrease in $\tilde{D}_S(t)$ at low frequency is even more prominent. For the sample with density $\rho^* = 0.581$, there is a cusp in the time dependence of $\tilde{D}_S(t)$. Over an intermediate range ($1485 > t > 726$ ms), $\tilde{D}_S(t)$ deviates positively from the $\ln(t)/t$ form. This ''enhanced mobility'' is most pronounced for $t \cong 660$ ms, the time previously identified with the long-range cooperative displacements that occur at this density. A similar cusp occurs for $\rho^* = 0.504$. In this case, however, the time corresponding to the maximum value of $\tilde{D}_S(t)$ ($t \cong 990$ ms) does not coincide with any obvious feature in the van Hove function. Just as in the case of the non-Gaussian parameter, the behavior of $\hat{D}_S(t)$ suggests that the time scale associated with at least one of the processes leading to the kinetic transition from random binary collisions (free motion) to structural arrest (hindered motion) scales inversely with increasing particle density. At the two lowest sample densities ($\rho^* = 0.241$ and 0.165), there is a gradual transition from free to hindered motion that precisely coincides with the deviation of $G_s(r,t)$ from Gaussian behavior.

IV. DISCUSSION

We have presented experimental evidence for the existence of stringlike cooperative motion in a quasi-two-dimensional liquid of uncharged spherical particles. Our experiments reveal the existence, in semidilute and dense liquid states, of a transition in the qualitative dynamical behavior of the system. At short times particles undergo unhindered Brownian motion, at intermediate times they undergo binary uncorrelated collisions, and at long times the self-diffusion mode is coupled to collective longitudinal acoustic modes of the fluid resulting in local fluctuating domains of enhanced particle mobility.

We studied the properties of these domains by examining the density dependence of the van Hove self-correlation function $G_s(r,t)$ and its deviation from Gaussian behavior. We observed that periods of non-Gaussian behavior correspond precisely to the timing of events involved in the relaxation of ''caged'' particles and their nearest neighbors. Our results are reminiscent of findings from molecular-dynamics simulations of glass-forming liquids carried out below the crystallization temperature. The presence of secondary peaks in $G_s(r,t)$ at intermediate times has been interpreted as evidence for an activated process in which a particle hops to one of the positions that was formerly occupied by one of the cage particles that initially surrounded it [5]. In the context of mode-coupling theory, this cage relaxation is associated with the α-relaxation process. More recent work has argued that non-Gaussian behavior of $G_s(r,t)$ specifically reflects the presence of dynamical heterogeneities in the system [3]. In the present work, direct comparison between the microscopic particle trajectories [Figs. 4(a) and 4(b)], the van Hove self-correlation function (Fig. 7), and the non-Gaussian parameter (Fig. 8) unambiguously shows that non-Gaussian behavior is indeed an indicator of dynamic heterogeneity. Furthermore, the lifetime of the dynamical heterogeneities (reflected in the peak position of α_2) is seen to shift towards shorter time scales with increasing particle density. One possible explanation for this observation is that the time scale associated with cage structural arrest in a colloidal fluid is correlated with the mean collision time experienced by a typical particle, $\langle \tau_{\text{collision}} \rangle = \langle l_{\text{sep}} \rangle^2 / D_0$. If this is so, the peak positions of the non-Gaussian parameter will depend on the density through the mean distance that particles must diffuse in order for their surfaces to undergo a collision, $\langle l_{\text{sep}} \rangle = \sigma[(1/\rho^*) - (\pi/4)]^{1/2}$. In Table V we list values for $\langle l_{\text{sep}} \rangle$ and $\langle \tau_{\text{collision}} \rangle$ as a function of particle density. We compare these values to estimates of the peak positions of $\alpha_2(t)$ based on the incomplete data displayed in Fig. 8. These values are roughly consistent with one another and we conclude that, for this system, the time scale associated with structural arrest appears to scale with the mean collision time. For the two highest densities, the values of $\langle \tau_{\text{collision}} \rangle$ fall at the beginning of the time window corresponding to the extended plateau in the mean-square displacement.

During the intermediate time range for which the system follows Gaussian behavior, the diffusion coefficient decays from its short-time ''free-particle'' value to its dressed value as $(\ln t)/t$, in agreement with the theoretical predictions of Cichocki and Felderhof [11]. This is true for all observed particle densities. The decay of the diffusion coefficient is

due to direct in-plane particle-particle collisions and is not a consequence of hydrodynamic interactions; the latter are important in determining the effective diffusion coefficient at shorter times and are included in the ''free-particle'' value. Our results indicate that the Gaussian approximation is an excellent representation of our system on time scales for which particle motion is uncorrelated and the dynamics appear homogeneous. When these conditions are met, the time dependence of the mean-square displacement may be obtained using Eq. (1.1). There is disagreement between our observations of the magnitude of the effect and the theoretical predictions. The observed magnitude is between two and ten times smaller than that predicted. The discrepancy is most likely due to the qualitative difference between the hard-core interaction used in both the Cichocki-Felderhof analysis and the Schofield-Marcus-Rice analysis and the colloid-colloid interaction in our real system. The latter interaction is inferred [8] to have a hard core, located at $R=\sigma$, a narrow ($\sim 0.01\sigma$) attractive well about $1k_BT$ deep, located at $\sim 1.06\sigma$, and a soft repulsion in the range $\sigma \leqslant R \leqslant 1.05\sigma$. Zangi and Rice [19] have shown that this colloid-colloid interaction reproduces the phase transitions reported by Marcus and Rice. Zangi and Rice also find that at high densities the character of the quasi-two-dimensional packing and phase transitions observed exhibits some sensitivity to the change from hard sphere to Marcus-Rice-type colloid-colloid interactions.

There are several reasons that we believe account for the discrepancies between the theoretical and experimental values. Foremost of these reasons is the fact that the theoretical analysis is primarily based on an oversimplified model of the direct particle interactions in which any attraction between colloid particles is neglected. The experiments clearly show evidence of quasibound states, even at low densities, which suggests that a non-negligible attractive component to the direct particle potential exists. Cichocki and Felderhof [11] have investigated the effect of direct attractive potentials on the dynamics of colloidal suspensions. They found that the attractive potential not only renormalizes the long-time self-diffusion coefficient but also leads to a more complicated dynamical picture in which the formation of bound pairs enters into the dynamical description and introduces an additional time scale.

Another probable cause of the discrepancy between experimental values and mode-coupling predictions of the long-time self-diffusion coefficient is due to the lack of detailed knowledge of the spectrum of collective excitations in colloidal systems. The mode-coupling effects depend rather sensitively on wave-vector cutoff values that define the range of the collective modes. These cutoff values, in turn, depend on knowledge of the density dependence of the short-time self-friction coefficient. For each system, this density dependence must either be measured experimentally or calculated from a theory incorporating the full hydrodynamic effects.

ACKNOWLEDGMENTS

This research was supported by a grant by the National Science Foundation. A.H.M. would like to acknowledge support from the University of Oregon. We thank Professor David Grier and John Crocker for the image analysis software. We have also benefited from funds by the National Science Foundation for Materials Research at the University of Chicago.

[1] M. Vergeles and G. J. Szamel, Chem. Phys. **110**, 3009 (1999); T. Pakula, Recent Res. Devel. In Polymer Sci. **1**, 101 (1996); M. G. Guenza, J. Chem. Phys. **110**, 7574 (1999).

[2] F. H. Stillinger and J. A. Hodgdon, Phys. Rev. E **50**, 2064 (1994); M. T. Cicerone and M. D. Ediger, J. Chem. Phys. **104**, 7210 (1996); M. T. Cicerone and M. D. Ediger, *ibid.* **103**, 5684 (1995); M. T. Cicerone, F. R. Blackburn, and M. D. Ediger, Macromolecules **28**, 8224 (1998); M. D. Ediger, C. A. Angell, and S. R. Nagel, J. Phys. Chem. **100**, 13 200 (1996).

[3] W. Kob, C. Donati, S. J. Plimpton, P. H. Poole, and S. C. Glotzer, Phys. Rev. Lett. **79**, 2827 (1997); C. Donati, J. F. Douglas, W. Kob, S. J. Plimpton, P. H. Poole, and S. C. Glotzer, *ibid.* **80**, 2338 (1998); M. M. Hurley and P. Harrowell, Phys. Rev. E **52**, 1694 (1995); M. M. Hurley and P. Harrowell, J. Chem. Phys. **105**, 10 521 (1996).

[4] I. M. de Schepper, J. J. van Loef, and A. F. E. M. Haffmans, J. Stat. Phys. **57**, 631 (1989).

[5] W. Kob and H. C. Andersen, Phys. Rev. E **51**, 4626 (1995); H. Lowen, J.-P. Hansen, and J.-N. Roux, Phys. Rev. A **44**, 1169 (1991); D. Thirmulai and R. D. Mountain, Phys. Rev. E **47**, 479 (1993).

[6] A. H. Marcus and S. A. Rice, Phys. Rev. Lett. **77**, 2577 (1996).

[7] A. H. Marcus, B. Lin, and S. A. Rice, Phys. Rev. E **53**, 1765 (1996).

[8] A. H. Marcus and S. A. Rice, Phys. Rev. E **55**, 637 (1997).

[9] B. Cichocki and B. U. Felderhof, J. Chem. Phys. **89**, 1049 (1988).

[10] B. Cichocki and B. U. Felderhof, J. Chem. Phys. **89**, 3705 (1988).

[11] B. Cichocki and B. U. Felderhof, J. Phys.: Condens. Matter **6**, 7287 (1994).

[12] J. Schofield, A. H. Marcus, and S. A. Rice, J. Phys. Chem. **100**, 18 950 (1996).

[13] J. C. Crocker and D. G. Grier, J. Colloid Interface Sci. **179**, 298 (1996).

[14] J.-P. Hansen and I. R. McDonald, *Theory of Simple Liquids* (Academic, London, 1986).

[15] B. R. A. Nijboer and A. Rahman, Physica (Amsterdam) **32**, 415 (1966); A. Rahman, Phys. Rev. A **136**, A405 (1964).

[16] A. H. Marcus, J. Schofield, and S. A. Rice (unpublished).

[17] J. Happel and H. Brenner, *Low Reynold's Number Hydrodynamics* (Kluwer, Dordrecht, 1963).

[18] B. J. Ackerson and L. J. Fleishman, J. Chem. Phys. **76**, 2675 (1982).

[19] R. Zangi and S. A. Rice, Phys. Rev. E **58**, 7529 (1998).